Journal of Clinical and Translational Hepatology **2026**
DOI: 10.14218/JCTH.2026.00429

Original Article

Mass Cytometry Reveals Cell Type-specific Immune Remodeling in Placentas of Women with Chronic Hepatitis B Infection

Zirong Yang[1,2#], Li Qi[2#], Yang Bai[1,2], Weiwei Zhou[3], Wenjing Wang[4], Yunxia Zhu[5*] and Junfeng Lu[1*]

[1]First Department of Liver Disease, Beijing You An Hospital, Capital Medical University, Beijing Institute of Hepatology, Beijing, China; [2]Department of Infectious Diseases, Affiliated Hospital of Shandong Second Medical University, Weifang, China; [3]Pediatric Department, Beijing You An Hospital, Capital Medical University, Beijing, China; [4]Beijing Institute of Hepatology, Beijing You An Hospital, Capital Medical University, Beijing, China; [5]Physical Examination Center, Beijing You An Hospital, Capital Medical University, Beijing, China

Received: May 29, 2026 | **Revised:** June 30, 2026 | **Accepted:** July 28, 2026 | **Published online:** August 26, 2026

Abstract

Background and Aims: Hepatitis B virus (HBV) vertical transmission remains a major health challenge, and the characteristics of the placental immune microenvironment in chronic infection remain unclear. This study aimed to use mass cytometry to comprehensively analyze phenotypic changes in placental immune cell subsets. ***Methods:*** We collected placental tissues from 20 pregnant women (6 healthy controls and 14 with chronic HBV infection). $CD45^+$ leukocytes were detected using a 35-marker antibody panel. Unsupervised clustering identified 14 clusters, of which 13 immune clusters were analyzed. ***Results:*** HBV mainly caused functional remodeling of placental immune cells rather than changes in cell composition ($P > 0.05$ for all subsets). In natural killer (NK) cells, CD38 ($P = 0.0020$) and CD16 ($P = 0.0020$) were notably upregulated and strongly correlated ($\rho = 0.872$, $P < 0.001$), suggesting potentially enhanced ADCC function. T cells showed upregulation of CD27, CD38, and CXCR5. Basophils exhibited the most pronounced changes: 9 differential markers (including chemokine receptors CCR4 and CCR7) were consistently downregulated. Classical monocytes showed an M1 polarization tendency (CD38↑, CD163↓). All *P*-values were raw; no markers remained significant after false discovery rate correction at an FDR threshold of < 0.1, indicating nominal significance. In addition, the coordinated expression patterns of markers within multiple cell subsets were weakened after infection. ***Conclusions:*** These exploratory findings suggest that HBV may reshape placental immunity through enhanced NK cell activation, broad basophil suppression, and disrupted marker coordination. The sample size was limited (n = 20), so the results need to be validated in larger cohorts. These findings provide new perspectives for understanding the mechanisms of mother-to-child transmission.

Citation of this article: Yang Z, Qi L, Bai Y, Zhou W, Wang W, Zhu Y, *et al*. Mass Cytometry Reveals Cell Type-specific Immune Remodeling in Placentas of Women with Chronic Hepatitis B Infection. J Clin Transl Hepatol 2026. doi: 10.14218/JCTH.2026.00429.

Introduction

Hepatitis B virus (HBV) infection has always been an extremely serious challenge in the global public health system. According to data from the 2021 Global Burden of Disease Study, approximately 283.64 million people (95% uncertainty interval, 260.11–307.69) were chronically infected with HBV in 2021.[1] Mother-to-child transmission (MTCT) remains the core mode of viral transmission in hepatitis B endemic areas.[2,3] Although the application of hepatitis B vaccine combined with immunoglobulin has greatly reduced the transmission rate, immunoprophylaxis failure still occurs in 5–10% of pregnant women with high viral loads.[3] As the core structure connecting the mother and fetus, the placenta has a unique immune microenvironment involving various immune cells; these cells must protect the fetus from pathogens while simultaneously avoiding immune rejection of the semi-allogeneic fetus.[4–7] Once this delicate balance is disrupted, it may lead to vertical transmission of pathogens or failure of immunoprophylaxis. Previous studies have shown that decidual natural killer (dNK) cells are the main immune cell population in the placenta, accounting for approximately 70% of decidual lymphocytes in early pregnancy and playing key roles in trophoblast invasion, vascular remodeling, and immune tolerance maintenance.[6,8,9] Other immune cell subsets in the placenta, including $CD56^{dim}$ $CD16^+$ natural killer (NK) cells, T cells, and monocytes/macrophages, are jointly involved in immune regulation and antimicrobial defense.[10]

Keywords: Hepatitis B virus; Chronic hepatitis B; Placenta; Pregnancy; Immune phenotyping; Natural killer cells; Basophils; Vertical transmission.

[#]Contributed equally to this work.

[*]**Correspondence to:** Junfeng Lu, First Department of Liver Disease, Beijing You An Hospital, Capital Medical University, Beijing Institute of Hepatology, NO. 8, Xitoutiao, You'anmenwai, Fengtai District, Beijing 100069, China. ORCID: https://orcid.org/0000-0003-0558-6816. Tel: +86-18201162190, Fax: +86-10-83997159, E-mail: junfengdoc@ccmu.edu.cn; Yunxia Zhu, Physical Examination Center, Beijing You An Hospital, Capital Medical University, NO. 8, Xitoutiao, You'anmenwai, Fengtai District, Beijing 100069 China. ORCID: https://orcid.org/0000-0002-1047-7035. Tel: +86-13693132583, Fax: +86-10-83997159, E-mail: zyx0718@ccmu.edu.cn.

Although basophils account for only a small proportion of peripheral blood leukocytes,[11] they can strongly produce Th2 cytokines and express a variety of chemokine receptors that regulate their migration; however, their role in the placental immune microenvironment has not been studied.[12] The functional state and migration ability of these immune cells are usually determined by the expression profiles of specific surface markers, such as CD38 (activation marker),[13] CD16 (mediator of cytotoxicity),[14] CD163 (monocyte polarization marker),[15] and chemokine receptors that regulate cell migration.[16] Recent studies have begun to reveal how HBV infection affects pregnancy immunity. Gao *et al*. found that HBV-infected pregnant women with high viral loads exhibited an increased proportion of effector/memory $CD8^+$ T cells and a distinct $CD8^+$ T-cell cluster (CD8-C2) with enhanced clonal expansion, indicating an activated but altered T-cell response.[17] Lin *et al*. showed that HBV X protein promotes viral replication in placental trophoblasts by degrading Smc5/6 and activating the EGFR/PI3K/AKT pathway, which inhibits trophoblast apoptosis and may increase the risk of intrauterine transmission.[18] However, whether chronic HBV infection alters the functional state and marker coordination of other placental immune cells (NK cells, T cells, monocytes, and basophils) remains unknown. To address this gap, we used mass cytometry (CyTOF) to perform high-dimensional single-cell analysis (simultaneously detecting 35 surface markers) on placental tissues from chronic HBV-infected and healthy pregnant women to systematically characterize HBV-induced changes in placental immune cell composition, functional marker expression, and expression coordination at the cell-type resolution, thereby providing new insights into the placental immune microenvironment.

Methods

Study design and participants

This study adopted a single-center, cross-sectional observational design, aiming to analyze the shaping effect of chronic HBV infection on the local immune microenvironment of the placenta with the help of mass cytometry (CyTOF).[19,20] The research team collected placental tissues from pregnant women with chronic HBV infection and from uninfected pregnant women at the time of delivery, prepared them into single-cell suspensions by enzymatic dissociation, and stained them with a metal antibody panel containing 35 markers. Immune cell populations were identified using an unsupervised clustering algorithm, and the expression levels of markers, proportions of cell subgroups, and co-expression patterns between markers were compared between the two groups of samples. This report was prepared with reference to the Strengthening the Reporting of Observational Studies in Epidemiology (STROBE) statement for cross-sectional studies.[21]

The recruitment and sample acquisition of participants were carried out at Beijing You An Hospital Affiliated to Capital Medical University from January 2024 to December 2025. This research protocol was officially approved by the Ethics Review Committee of the hospital (Approval No.: LL-2024-001-K). Before sample collection, all enrolled pregnant women signed a written informed consent form, and all research procedures strictly followed the ethical guidelines of the Declaration of Helsinki.[22]

A total of 20 pregnant women were included in the analysis, including 6 healthy controls (HD group) and 14 HBV-infected pregnant women (PA group). The inclusion criteria for the PA group were as follows: HBsAg positivity with a disease course of more than 6 months,[23] singleton pregnancy, full-term delivery (gestational age ≥ 37 weeks), complete medical records (covering the five HBV serological indicators [HBsAg, anti-HBs, HBeAg, anti-HBe, and anti-HBc], HBV DNA quantification, liver function, routine blood tests, and prenatal hepatobiliary ultrasound), delivery completed in our hospital, and signed informed consent. The inclusion criteria for the HD group were as follows: negative HBsAg, HBeAg, anti-HBc, and anti-HBe results (anti-HBs status was not restricted to include healthy individuals who had previously received hepatitis B vaccination), singleton pregnancy, full-term delivery (gestational age ≥ 37 weeks), complete medical records, and signed informed consent. The common exclusion criteria for both groups included co-infection with HCV, HDV, HEV, HIV, or Treponema pallidum; long-term use of glucocorticoids or other immunosuppressive drugs; prenatal diagnosis of fetal congenital malformations; gestational diabetes or preeclampsia; chorioamnionitis or other placental pathological changes; and a history of autoimmune diseases.

The basic demographic characteristics, obstetric indicators, and HBV virological status of the enrolled population are summarized in Table 1.

Sample collection and placental tissue processing

To obtain a placental immune single-cell suspension suitable for mass cytometry analysis, placental tissue was retrieved immediately after delivery of the fetus.[24] The sampling site was selected from the central villous area on the maternal side of the placenta near the umbilical cord insertion site, with a size of approximately 1–2 cm^3. During the procedure, calcification foci, infarct areas, maternal decidua, and the chorionic plate were carefully avoided.[24,25] To reduce potential maternal blood contamination, the tissue blocks were repeatedly rinsed with pre-cooled PBS before enzymatic dissociation until no visible blood remained.[26] The tissue block was quickly immersed in pre-cooled Dulbecco's Modified Eagle Medium (DMEM) to ensure that the time from separation to processing did not exceed 2 h.[24]

Enzymatic tissue dissociation: Placental tissue dissociation was performed using a gentleMACS Dissociator equipped with a heater sleeve (Miltenyi Biotec, Bergisch Gladbach, Germany) and the Human Tumor Dissociation Kit (Miltenyi Biotec; cat. no. 130-095-929), following the manufacturer's protocol.[27] The enzyme working solution was prepared as follows: 4.7 mL DMEM, 200 µL Enzyme H, 100 µL Enzyme R, and 25 µL Enzyme A were added sequentially to a gentleMACS C Tube (Miltenyi Biotec) and mixed thoroughly. The placental sample was cut into small pieces approximately 2–4 mm in size using sterile scissors; adipose tissue, fibrous bundles, and visible necrotic areas were carefully removed during this step. The treated tissue fragments were then transferred to the C Tube containing the enzyme mixture.

The C Tube was capped, inverted, and loaded onto the preheated gentleMACS Dissociator so that the tissue fragments fell into the rotor–stator region. After attaching the heater sleeve, the built-in program "37C_h_TDK_2" (for medium-density placental tissue) was selected and run for 20 min. After the program was completed, the C Tube was removed and briefly centrifuged to collect the dissociated material at the bottom of the tube. The pellet was resuspended by pipetting, and the resulting cell suspension was filtered into a 50 mL conical tube through a 70 µm SmartStrainer (Miltenyi Biotec, Bergisch Gladbach, Germany; cat. no. 130-098-462).[26] Finally, the strainer was washed repeatedly with 30 mL of PBS to maximize recovery of released cells.

Red blood cell lysis and cell preparation: To further

Table 1. Clinical characteristics of study participants

Characteristic	HD (n = 6)	PA (n = 14)	*P*-value
Demographics			
Age (years), mean ± SD	31.3 ± 2.2	31.5 ± 2.8	0.931
Obstetric			
Gestational age (weeks), mean ± SD	39.5 ± 0.7	39.4 ± 1.1	0.837
Cesarean delivery, n (%)	3 (50.0)	7 (50.0)	1
Metabolic			
Fasting glucose (mmol/L), mean ± SD	4.30 ± 0.33	4.38 ± 0.33	0.592
Liver function			
ALT (U/L), mean ± SD	12.8 ± 3.5	15.4 ± 7.4	0.427
AST (U/L), mean ± SD	22.3 ± 7.2	27.8 ± 12.0	0.225
HBV serological status			
HBsAg (IU/mL), median (range)	–	5,800 (1,165–67,349)	–
HBeAg positive, n (%)	–	6 (42.9)	–
HBeAg negative, n (%)	–	8 (57.1)	–
HBV status			
HBV DNA < 1,000 IU/mL, n (%)	–	8 (57.1)	–
HBV DNA ≥ 1,000 IU/mL, n (%)	–	6 (42.9)	–
Antiviral therapy during pregnancy			
Tenofovir disoproxil fumarate (TDF), n (%)	–	10 (71.4)	–
No antiviral therapy, n (%)	–	4 (28.6)	–
Median initiation (gestational weeks)	–	27 (pre-pregnancy to 32)	–

Data are presented as mean ± SD for normally distributed continuous variables, median (range) for skewed variables, and n (%) for categorical variables. HBV-related characteristics are shown for the PA group only. All TDF-treated patients received 300 mg once daily. HD, healthy donors; PA, HBV-infected pregnant women; SD, standard deviation; ALT, alanine aminotransferase; AST, aspartate aminotransferase; HBsAg, hepatitis B surface antigen; HBeAg, hepatitis B e antigen; TDF, tenofovir disoproxil fumarate.

remove residual maternal erythrocytes and any circulating leukocytes potentially trapped in the placental vasculature, a red blood cell lysis step was performed. The collected cell suspension was centrifuged at 300 × g for 5 min at room temperature, and the supernatant was carefully aspirated. To remove residual red blood cells, the pellet was resuspended in 1× Red Blood Cell Lysis Buffer (Solarbio, Beijing, China; cat. no. R1010) and incubated at room temperature for 6 min.[26] Then, 2 volumes of 5% fetal bovine serum (FBS; Gibco, Grand Island, NY, USA; cat. no. A5669701) in PBS were immediately added to stop the lysis reaction. The mixture was centrifuged at 500 × g for 5 min, the supernatant was discarded, the pellet was rinsed with 15 mL PBS, equally divided into two centrifuge tubes, and then pelleted again under the same conditions (500 × g for 5 min), after which the supernatant was removed.

Sample cryopreservation: One aliquot was used for live-cell cryopreservation in 1 mL CELLSAVING serum-free freezing medium (NCM Biotech, Suzhou, Jiangsu, China; cat. no. C40100) and transferred to a liquid nitrogen tank for long-term preservation in preparation for subsequent functional verification.[28] The other aliquot was used for mass cytometry analysis. To distinguish live from dead cells, cisplatin covalent labeling was performed as a viability indicator for mass cytometry.[19,29] Specifically, 1 mL of 0.01% cisplatin solution (Standard Biotools, South San Francisco, CA, USA; cat. no. 201064) was added to the sample, gently mixed, and incubated at room temperature for 2 min according to the manufacturer's recommended protocol.[29] The treated cells were rinsed once with 5% FBS in PBS, centrifuged at 500 × g for 5 min, and the supernatant was aspirated. The cells were then fixed at room temperature with 500 μL of 1× Fix I Buffer (diluted from 5× Maxpar Fix I Buffer; Standard Biotools, South San Francisco, CA, USA; cat. no. 201065) for 15 min.[30] After fixation, 1 mL of 5% FBS in PBS was added to terminate the reaction. The sample was centrifuged at 500 × g for 5 min, and the supernatant was discarded. Finally, the pellet was resuspended in 1 mL of cell staining buffer (CSB, namely 10% DMSO [Sigma-Aldrich, St. Louis, MO, USA; cat. no. D2650] dissolved in DPBS [Servicebio, Wuhan, Hubei, China; cat. no. G4200-500ML]), transferred to −80 °C for freezing and preservation, and stored until uniform batch acquisition.[30]

Metal antibody conjugation

To achieve the simultaneous detection of 35 surface markers, commercially available purified antibodies were labeled with lanthanide metals using the Maxpar X8 Multi-Metal Labeling Kit (Standard Biotools, South San Francisco, CA, USA; cat. no. 201300), following the protocol previously established for mass cytometry antibody conjugation.[19,30] The labeling was performed strictly according to the manufacturer's instructions.[30] As this kit is a validated commercial labeling system, the labeling efficiency has been verified by the manufacturer, and the included W-Buffer washing steps are designed to remove free metal residues; therefore, no additional in-house

validation was required.

To completely dissolve the polymer, we first added 95 μL of L-Buffer to the X8-polymer tube and performed vortexing. Then, 5 μL of lanthanide metal stock solution (50 mM) was added and mixed. After thorough mixing, the mixture was placed in a 37 °C water bath for 30 min. At the same time, 100 μg of target antibody was added to an ultrafiltration tube with a molecular weight cutoff of 50 kDa (Amicon Ultra, MilliporeSigma, Burlington, MA, USA; cat. no. UFC5050BK), brought to 400 μL with R-Buffer, and centrifuged at 12,000 × g for 10 min at room temperature.[30]

The TCEP reducing agent (Thermo Fisher Scientific, Waltham, MA, USA; cat. no. T2556) was diluted 1:100 with R-Buffer to prepare a 4 mM working solution for later use.[31] A total of 200 μL of L-Buffer was pre-added to a 3 kDa ultrafiltration tube (Amicon Ultra, MilliporeSigma, Burlington, MA, USA; cat. no. UFC5003BK), and the above metal–polymer reaction liquid was then transferred onto the 3 kDa membrane and centrifuged at 12,000 × g for 30 min at room temperature to purify the metallized polymer. To fully expose the thiol groups of the antibody hinge region, 100 μL of 4 mM TCEP working solution was added to the 50 kDa ultrafilter containing the antibodies. After rapid mixing, the sample was immediately transferred to a 37 °C environment and incubated for 30 min to complete the reduction reaction.[30]

After centrifugation, the waste liquid at the bottom of the 3 kDa collection tube was discarded. Then, 400 μL of C-Buffer was added, and the centrifuge tube was placed at room temperature and continuously centrifuged for 30 min at 12,000 × g to achieve buffer exchange. Next, 300 μL of C-Buffer was added to the 50 kDa ultrafilter, and the tube wall was gently rinsed by pipetting to recover any adsorbed antibody, followed by centrifugation at 12,000 × g for 10 min. The waste liquid was discarded, and 400 μL of C-Buffer was added to repeat the washing step, followed by centrifugation for 10 min under the same conditions. After completing the above steps, the 3 kDa filter assembly was removed first, followed by the 50 kDa assembly, and the metal isotope number corresponding to each antibody was checked individually. A total of 60 μL of C-Buffer was added to the 50 kDa membrane, and the entire purified metal–polymer solution was gently mixed by pipetting and transferred onto the 50 kDa membrane. The assembly was placed in a 37 °C water bath for 90 min to complete the covalent conjugation between the polymer and the antibody.[30]

At the end of the conjugation process, 300 μL of W-Buffer was added to the 50 kDa filter membrane, followed by centrifugation at 12,000 × g for 10 min at room temperature. To ensure complete removal of free metal, the waste liquid was discarded, and the above washing procedure was repeated three times using the same volume of W-Buffer.[30] After washing, 100 μL of antibody stabilizer (Candor Bioscience, Wangen im Allgäu, Germany; cat. no. 131050) was added.[32] The filter unit was then placed upside down into a new collection tube and centrifuged at 1,000 × g for 2 min at room temperature to elute the target product.[30] The prepared metal-conjugated antibodies were stored at 4 °C for subsequent use.[32]

CyTOF antibody panel

To systematically depict the phenotypic spectrum of placental immune cells, we designed a custom panel of metal-conjugated antibodies covering 35 surface antigens (see Table 2 for details).[33] The selected markers involved multiple functional dimensions[34]: lineage identification (CD3, CD4, CD8, CD19, CD56, CD14, CD66B, TCRγδ); immune activation status (CD38, HLA-DR, CD25, CD27, CD28); differentiation and maturation (CD45, CD45RA, CD45RO, CD57, CD127); cytotoxic effector function (CD16, granzyme B); migration and chemokine receptors (CD183, CD185, CD194, CD196/CCR6, CD197, CD294/CRTH2); myeloid markers (CD11B, CD11C, CD68, CD123, CD163); adhesion molecules (CD31, CD105, αSMA); and other related molecules (CD24, CD56). The antibodies used in this study were divided into two categories: one category was directly purchased from commercial suppliers as pre-conjugated reagents, whereas the other was labeled in-house from commercially available purified antibodies using the Maxpar X8 Multi-Metal Labeling Kit, strictly following the manufacturer's instructions as described in Section 2.3.[30]

Metal-conjugated antibody labeling of placental leukocytes

Before the staining experiment, cryopreserved cells were placed at 37 °C for rapid thawing and then rinsed with 5% FBS in DPBS. During the barcode labeling step, the recovered leukocytes were first mixed with Barcode Perm buffer (Standard Biotools, South San Francisco, CA, USA), followed by centrifugation at 800 × g for 5 min; the washing step was performed for two consecutive rounds. Subsequently, each tube of the 20-Plex Pd Barcoding Kit (Standard Biotools, South San Francisco, CA, USA; cat. no. 201060) was reconstituted with 100 μL of Barcode Perm. After brief vortexing, the solution was mixed individually with the corresponding leukocyte sample according to the preset barcoding scheme[35] and incubated at room temperature in the dark for 30 min.[36]

After the reaction, 1 mL of 5% FBS in DPBS was added to quench the barcode labeling, and the sample was centrifuged at 800 × g for 5 min. The pellet was rinsed twice with the same buffer and finally resuspended in 100 μL of 5% FBS in DPBS. All barcoded samples were then pooled into a single reaction system. After centrifugation at 800 × g for 5 min, the metal–antibody mixture prepared according to Table 2 was added and incubated at room temperature in the dark for 30 min. At the end of incubation, the sample was rinsed once with 1 mL of 5% FBS in DPBS and centrifuged at 800 × g for 5 min to remove unbound antibodies.[30]

To fix the stained white blood cells, 1 mL of Fix I Buffer (Standard Biotools, South San Francisco, CA, USA; cat. no. 201065) was added and mixed thoroughly, followed by centrifugation at 800 × g for 5 min. The collected cell pellet was washed twice consecutively with 1 mL of DPBS and then resuspended in 100 μL of DPBS containing 5% FBS. After gentle vortexing, 500 μL of 0.1% Cell-ID Intercalator-Ir (Standard Biotools, South San Francisco, CA, USA; cat. no. 201192A) was added, and the sample was incubated overnight at 4 °C to achieve DNA labeling.[20,33] On the day of data acquisition, the white blood cells were washed three times with ultrapure water and then resuspended in cell acquisition solution containing 10% EQ Four Element Calibration Beads (Standard Biotools, South San Francisco, CA, USA; cat. no. 201078).[37] Finally, the mixture was filtered through a 40 μm cell strainer (Corning, Corning, NY, USA; cat. no. 352340) and immediately placed in an ice bath to await data acquisition.

CyTOF data acquisition

The acquisition of single-cell proteomic data was completed at the Beijing Institute of Hepatology, Beijing You An Hospital Affiliated with Capital Medical University. The instrument used was a Helios mass cytometer (Standard Biotools, South San Francisco, CA, USA). Before each run, the instrument was tuned and calibrated according to the standard operat-

Table 2. Mass cytometry antibody panel for placental immune cell phenotyping

Antigen	Symbol and mass	Antibody clone	Source	Catalog number
CD127	141Pr	A019D5	Polaris	H03612094-25T
CD194	142Nd	L291H4	Polaris	H09521095-25T
CD196	143Nd	G034E3	Polaris	H09711096-25T
CD31	144Nd	WM59	Fluidigm	3144023C
ASMA	145Nd	1A4	Abcam	ab240654
CD27	146Nd	O323	Polaris	H14923099-25T
CD45RO	147Sm	UCHL1	Polaris	H21612105-25T
CD57	148Nd	REA769	Polaris	H23542100-25T
CD28	149Sm	CD28.2	Polaris	H15911107-25T
CD105	150Nd	EPR22811-18	Abcam	ab256146
HLA_DR	151Eu	L243	Polaris	H31111111-25T
CD8	152Sm	SK1	Polaris	H25754109-25T
CD45RA	153Eu	HI100	Polaris	H21411112-25T
CD123	154Sm	6H6	Polaris	H03311110-25T
CD294	155Gd	BM16	Polaris	H16511115-25T
CD183	156Gd	G025H7	Polaris	H08912116-25T
CD11C	158Gd	Bu15	Polaris	H03112118-25T
CD16	159Tb	CB16	Polaris	H06767120-25T
CD19	160Gd	HIB19	Polaris	H09212119-25T
CD24	161Dy	REA832	Polaris	H13132124-25T
CD185	162Dy	J252D4	Polaris	H09131125-25T
CD25	163Dy	M-A251	Polaris	H13553126-25T
CD14	164Dy	UCHM1	Polaris	H04842127-25T
CD66B	165Ho	6/40c	Polaris	H24832128-25T
CD56	166Er	NCAM16.2	Polaris	H23414131-25T
CD197	167Er	G043H7	Polaris	H09813132-25T
CD4	168Er	OKT-4	Polaris	H20631133-25T
CD68	169Tm	KP1	Abcam	ab233172
CD38	170Er	HIT2	Polaris	H20412134-25T
CD45	171Yb	BC8	Polaris	H21231138-25T
CD11B	172Yb	SP330	Abcam	ab241408
GB	173Yb	RM1165	Abcam	ab317459
TCRyd	174Yb	REA591	Polaris	H40762141-25T
CD163	175Lu	EPR19518	Abcam	ab213612
CD3	209Bi	UCHT-1	Polaris	H16712189-25T

αSMA, alpha-smooth muscle actin; CCR, C-C chemokine receptor; CRTH2, chemoattractant receptor-homologous molecule expressed on Th2 cells; CXCR, C-X-C chemokine receptor; HLA-DR, human leukocyte antigen-DR; TCR, T-cell receptor.

ing procedures provided by the manufacturer.[36] Each sample yielded at least 1×10^5 events, and the acquisition rate was controlled between 300 and 500 events per second to balance sensitivity and signal stability.[30,36]

Data processing and quality control

To ensure data quality and remove technical artifacts, the raw CyTOF data were first processed using CyTOF Software v7.0 (Standard Biotools). Based on the EQ Four Element calibration bead signals, signal drift during acquisition of the original FCS (Flow Cytometry Standard) files was corrected, and standardized FCS files were generated.[36,37] The CyTOF Debarcoding Tool was then used to deconvolute the pooled samples individually according to the preset barcoding scheme.[35]

The debarcoded data were uploaded to the Cytobank online platform (https://www.cytobank.org) for subsequent quality control and preprocessing.[38,39] Specifically, EQ bead

signals were first eliminated, and debris and cell aggregates were filtered out according to event length parameters. Non-viable cells were excluded based on high cisplatin uptake signals (a characteristic of dead cells with impaired membrane integrity), and $CD45^+$ events were retained through gating for downstream analysis.[39] The cleaned FCS files were then exported for computational analysis. All marker expression values were processed using an arcsinh transformation with a cofactor of 5 as input for subsequent analysis.[33,36] Because cells were fixed with Fix I Buffer before storage, conventional viability dyes could not be applied, and the cisplatin signal served as the standard viability indicator in mass cytometry.[29] The same processing and gating procedures were applied to all samples in both groups.

Unsupervised clustering and cell population identification

To identify various immune cell populations without prior bias, the cytofkit package (https://bioconductor.org/packages/cytofkit/) was called within the R environment to perform unsupervised clustering of $CD45^+$ events.[40] Cluster computation was performed using the PhenoGraph algorithm,[41] and UMAP (Uniform Manifold Approximation and Projection) was used for dimensionality reduction and projection to facilitate visualization of cellular heterogeneity on a two-dimensional plane.[42]

Each cluster was then manually annotated according to classical marker expression profiles. The specific rules were as follows: NK cell subgroups were defined as $CD56^+CD3^-$ populations and further subdivided according to CD16, CD38, and CD57 expression; T cell subgroups were defined as $CD3^+$ populations and divided according to CD4/CD8 expression, CD45RA/CD45RO status, and activation markers; B cells were defined as $CD19^+CD3^-$ populations; monocyte populations were defined as $CD14^+$ populations and divided into classical ($CD14^{++}CD16^-$) and intermediate ($CD14^{++}CD16^+$) subsets according to CD16 expression; neutrophils were identified as $CD66B^+$ cells, and basophils were identified as $CD123^+$HLA-DR^- cells.[34] A total of 14 clusters were obtained during preliminary clustering. Cluster 14 was excluded from subsequent analysis because it showed simultaneous high expression of CD3 (a T-cell marker) and CD66B (a neutrophil marker). Since T cells and neutrophils belong to different lineages and do not normally co-express these markers, this pattern most likely reflected cell doublets or technical artifacts rather than a true biological cell population.[39]

Statistical analysis

Sample size consideration: This study was exploratory in nature, and its purpose was to generate new scientific hypotheses rather than conduct confirmatory significance testing. Given the limited sample size (HD group, n = 6; PA group, n = 14), the study had modest statistical power (approximately 34.2% under a two-sided $\alpha = 0.05$ for a large effect size, Cohen's $d = 0.8$).[43] Therefore, effect size estimation was used together with *P*-values to interpret between-group differences.

Comparison of cell population proportions: The proportion of each cluster was defined as the percentage of cells in that cluster relative to the total $CD45^+$ events in the sample. Given the non-normal distribution of the data and the small sample size, comparisons of proportions between the HD and PA groups were uniformly performed using the two-sided Mann–Whitney U test.[39]

Differential marker expression analysis: For the 13 immune cell clusters, the Mann–Whitney U test was applied individually to evaluate differences in the median expression levels of 35 surface markers between the HD and PA groups.[39] The fold change (FC) was defined as the ratio of the mean value in the PA group to that in the HD group. The entire analysis generated a total of 455 pairwise comparisons (13 clusters × 35 markers).

Multiple testing correction: In this study, statistical significance was defined as a false discovery rate (FDR) < 0.1. All raw *P*-values from multiple comparisons were adjusted using the Benjamini–Hochberg method.[44,45] Given the exploratory nature of this study, markers satisfying $P < 0.05$ without correction were also listed as candidate differential markers for reference in subsequent hypothesis generation; however, caution should be exercised when interpreting these findings.

Effect size calculation: At the same time, Cohen's d and its 95% confidence interval were calculated to measure the actual magnitude of between-group differences independent of sample size. The interpretation criteria for effect sizes were as follows: negligible ($|d| < 0.2$), small effect ($0.2 \leq |d| < 0.5$), medium effect ($0.5 \leq |d| < 0.8$), and large effect ($|d| \geq 0.8$).[43]

Correlation analysis: To explore whether synergistic interactions existed between key markers within specific cell clusters, we employed the Spearman rank correlation coefficient for evaluation. Correlations were calculated under three sample configurations: pooled samples (n = 20), HD group alone (n = 6), and PA group alone (n = 14), to determine whether HBV infection altered the coordinated expression patterns between functionally related molecules.

Statistical software: All statistical analyses were performed in the R 4.5.0 environment (R Foundation for Statistical Computing, Vienna, Austria). The main R packages used included cytofkit,[40] flowCore, ggplot2, and dplyr. In addition, the Sangerbox online platform (http://www.sangerbox.com)[46] and GraphPad Prism 10.2.0 software (GraphPad Software, San Diego, CA, USA) were used for downstream analyses, including cell cluster composition evaluation, protein expression quantification, and correlation visualization. In all individual comparisons, two-sided $P < 0.05$ was used as the threshold for statistical significance.

Results

Clinical characteristics of study participants

Table 1 lists the clinical characteristics of all participants in each group in detail. The two groups were comparable in terms of age (HD: 31.3 ± 2.2 years; PA: 31.5 ± 2.8 years; $P = 0.931$), gestational age at delivery (HD: 39.5 ± 0.7 weeks; PA: 39.4 ± 1.1 weeks; $P = 0.837$), mode of delivery (cesarean section: HD 50.0%; PA 50.0%; $P = 1.000$), and fasting glucose levels (HD: 4.30 ± 0.33 mmol/L; PA: 4.38 ± 0.33 mmol/L; $P = 0.592$). Liver function tests (ALT and AST) were within the normal range in both groups. Among the PA group, 6 cases (42.9%) were HBeAg-positive and had high viral loads (HBV DNA ≥ 1,000 IU/mL), while the remaining 8 cases (57.1%) were HBeAg-negative with low viral loads (HBV DNA < 1,000 IU/mL). Ten cases (71.4%) received tenofovir disoproxil fumarate (TDF) antiviral therapy during pregnancy, with a median initiation time of 27 gestational weeks (range: pre-pregnancy to 32 weeks).

Identification of placental immune cell populations

We performed unsupervised clustering analysis on $CD45^+$ leukocytes isolated from 20 placental tissue samples (HD group, n = 6; PA group, n = 14) and identified a total of 14 cell clusters. UMAP dimensionality reduction visualization

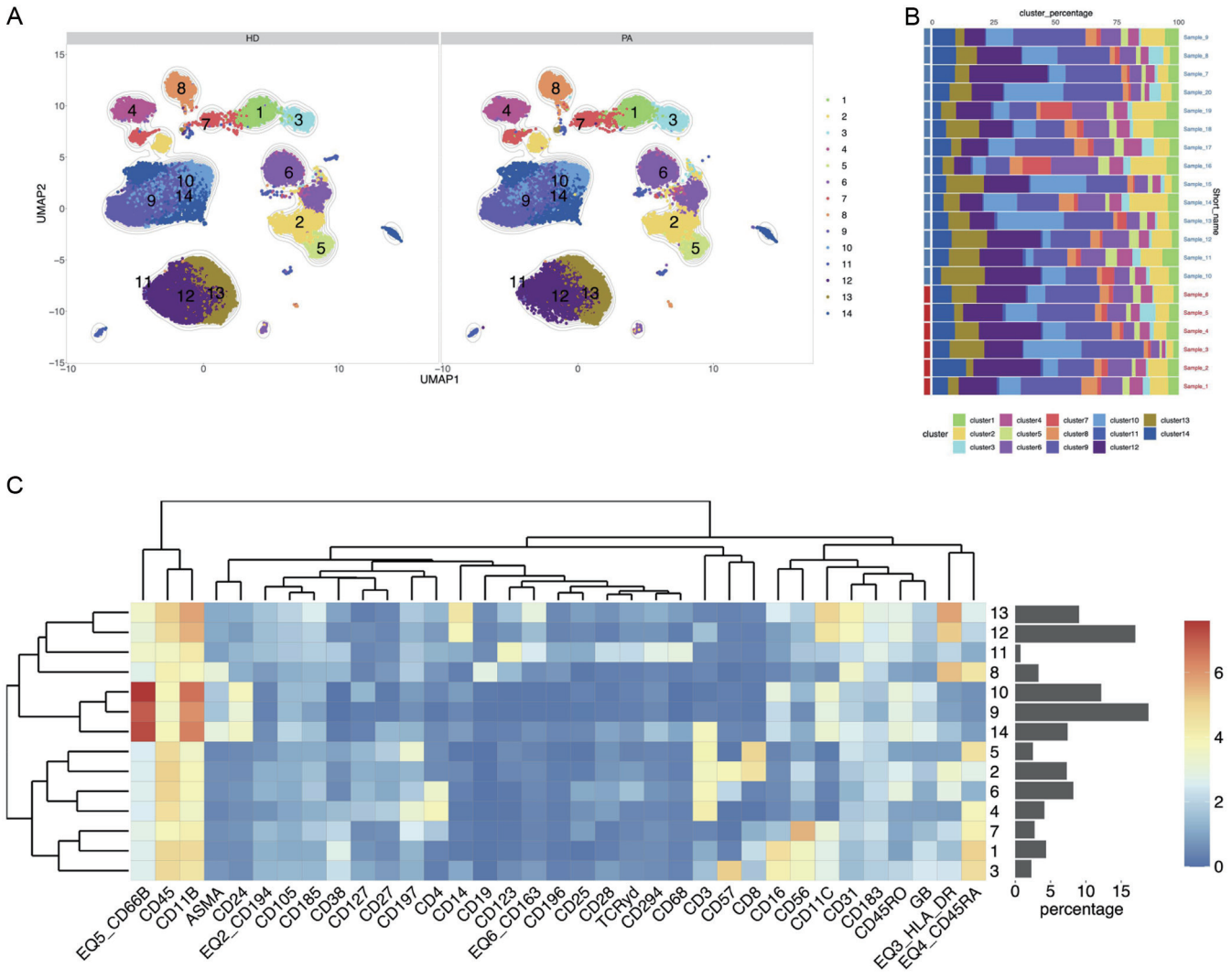

Fig. 1. Identification and characterization of immune cell populations in placental tissues. (A) UMAP visualization of 14 cell clusters identified by unsupervised clustering of CD45$^+$ cells from placental tissues. The left panel shows cells colored by cluster identity; the right panels show the distribution of cells from the HD and PA groups separately. (B) Stacked bar chart showing the proportional composition of 14 cell clusters in each sample. Samples are grouped by HD (left) and PA (right). Colors correspond to cluster identities as shown in panel A. (C) Heatmap displaying the expression profiles of canonical markers across 14 cell clusters. Color intensity represents mean expression level (arcsinh-transformed). Markers are grouped by functional categories. Cluster annotations are shown at the bottom. HD, n = 6; PA, n = 14. UMAP, Uniform Manifold Approximation and Projection; HD, healthy donors; PA, HBV-infected pregnant women; NK, natural killer cells.

showed that there was a similar cell distribution pattern between the HD and PA groups, and all cell clusters existed in both groups (Fig. 1A).

The 14 cell clusters were annotated according to canonical marker expression profiles (Fig. 1C). Clusters 1, 3, and 7 were NK cell subsets: Cluster 1 (CD38^{hi} CD56^{dim} CD16$^+$ NK), Cluster 3 (CD56^{dim} CD16$^+$ CD57$^+$ mature NK), and Cluster 7 (CD56^{bright} NK). Clusters 2 and 4–6 were T cell subsets: Cluster 2 (activated late-differentiated CD8 T cells), Cluster 4 (naive CD4 T cells), Cluster 5 (naive CD8 T cells), and Cluster 6 (activated CD4 effector memory-like T cells). Cluster 8 was identified as B cells. Clusters 9–13 were myeloid cells: Cluster 9 (neutrophils), Cluster 10 (mature neutrophils), Cluster 11 (basophils), Cluster 12 (classical monocytes), and Cluster 13 (intermediate monocytes). Based on the aberrant co-expression patterns of CD3 and neutrophil markers, as well as event characteristics, Cluster 14 was identified as doublets/artifacts and excluded from subsequent analyses.

The proportional distribution of cell clusters across individual samples (Fig. 1B) demonstrated that myeloid cells (Clusters 9, 10, 12, and 13) constituted a large proportion of cells in all samples, while inter-individual variation in cell composition was observed.

Analysis of cell population proportions

After excluding Cluster 14, the remaining 13 immune cell subsets were compared between groups. Myeloid cells were the predominant immune cell type in placental tissues from both groups. Neutrophils (HD: 23.4 ± 3.9%; PA: 19.2 ± 6.7%), classical monocytes (HD: 22.0 ± 6.4%; PA: 16.5 ± 7.5%), and mature neutrophils (HD: 12.3 ± 6.9%; PA: 12.7 ± 8.3%) collectively accounted for more than 50% of total CD45$^+$ leukocytes (Table 3; Fig. 2A).

Statistical comparison of cell subset proportions between the HD and PA groups revealed no significant differences

Table 3. Comparison of immune cell populations in placental tissues between HD and PA

Category	Cell population	HD (n = 6)	PA (n = 14)	Fold change	*P*-value	Cohen's d (95% CI)
Myeloid cells	Classical monocytes	21.97 ± 6.38	16.46 ± 7.49	0.75	0.127	−0.76 [−1.75, 0.22]
Myeloid cells	Intermediate monocytes	8.14 ± 4.78	9.96 ± 4.80	1.22	0.386	0.38 [−0.59, 1.34]
Myeloid cells	Neutrophils	23.44 ± 3.93	19.18 ± 6.65	0.82	0.149	−0.71 [−1.69, 0.28]
Myeloid cells	Mature neutrophils	12.28 ± 6.85	12.73 ± 8.25	1.04	1.000	0.06 [−0.90, 1.01]
Myeloid cells	Basophils	0.91 ± 0.32	0.75 ± 0.28	0.83	0.386	−0.52 [−1.49, 0.45]
T cells	Naive CD4 T cells	4.35 ± 1.45	4.88 ± 1.52	1.12	0.650	0.35 [−0.61, 1.32]
T cells	Naive CD8 T cells	2.26 ± 0.87	2.97 ± 1.16	1.31	0.303	0.65 [−0.33, 1.63]
T cells	Activated CD4 Tem-like	7.75 ± 2.86	9.51 ± 4.26	1.23	0.386	0.45 [−0.52, 1.42]
T cells	Activated late-diff CD8 T	6.76 ± 2.36	8.52 ± 4.41	1.26	0.536	0.45 [−0.52, 1.41]
NK cells	$CD56^{bright}$ NK	2.01 ± 0.65	3.73 ± 3.99	1.86	0.711	0.50 [−0.47, 1.48]
NK cells	$CD38^{hi}$ $CD56^{dim}$ $CD16^{+}$ NK	4.05 ± 1.39	4.94 ± 2.05	1.22	0.592	0.47 [−0.50, 1.44]
NK cells	$CD56^{dim}$ $CD16^{+}$ $CD57^{+}$ mature NK	2.27 ± 2.52	2.71 ± 1.84	1.19	0.386	0.21 [−0.74, 1.17]
B cells	B cells	3.80 ± 1.69	3.65 ± 1.70	0.96	0.837	−0.09 [−1.04, 0.87]

Data are presented as mean ± SD and expressed as percentages of total $CD45^{+}$ cells. Fold change was calculated as PA mean / HD mean; values >1 indicate higher proportions in the PA group. Effect size categories: large (|d| ≥ 0.8), medium (0.5 ≤ |d| < 0.8), small (0.2 ≤ |d| < 0.5), negligible (|d| < 0.2). CI, confidence interval; diff, differentiated; HD, healthy donors; NK, natural killer cells; PA, HBV-infected pregnant women; Tem, effector memory T cells.

(Mann–Whitney U test, all $P > 0.05$; Fig. 2B; Supplementary Table 1). Effect size analysis showed that five cell subsets exhibited medium or larger effect sizes (|d| ≥ 0.5), including classical monocytes (d = −0.76), neutrophils (d = −0.71), and naive CD8 T cells (d = 0.65); however, all 95% confidence intervals crossed zero (Fig. 2C). Post hoc power analysis demonstrated that the current sample size had 34.2% power to detect large effects (d = 0.8) (Supplementary Fig. 1A; Supplementary Table 2).

Overview of differential marker expression analysis

Systematic differential expression analysis was performed for 35 surface markers across 13 immune cell subsets, totaling 455 statistical comparisons. Fifty-five comparisons (12.1%) showed nominal differences at raw $P < 0.05$, of which 13 reached raw $P < 0.01$. After Benjamini–Hochberg FDR correction, no markers reached the significance threshold of FDR < 0.1; therefore, all marker-level differences reported hereafter are based on uncorrected raw *P*-values and should be interpreted as candidate signals. Among the 55 candidate differential markers with nominal significance (raw $P < 0.05$), 31 (56.4%) were upregulated in the PA group, while 24 (43.6%) were downregulated (Supplementary Table 3; Fig. 3A).

Analysis by functional marker categories (Fig. 3B; Supplementary Table 4) showed that migration-related markers exhibited the most differences (15, ↑9/↓6), followed by T cell lineage markers (8), activation markers (6, ↑5/↓1), and myeloid markers (6). All four differences in cytotoxicity-related markers were upregulated, and five of six activation markers showed upregulation (Supplementary Fig. 1B).

Different cell subsets displayed varying degrees and directions of marker expression changes (Supplementary Table 5; Supplementary Fig. 2A). Basophils (Cluster 11) showed the most differentially expressed markers (9, all downregulated), followed by mature neutrophils (Cluster 10, 7, 6↓/1↑) and classical monocytes (Cluster 12, 6, 1↑/5↓). NK cell and T cell subsets predominantly showed marker upregulation.

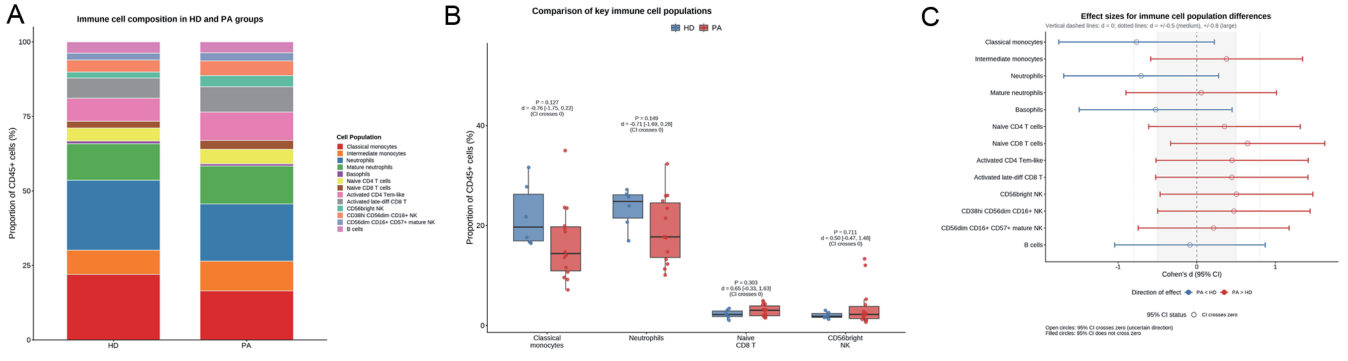

Fig. 2. Comparison of immune cell population proportions between HD and PA groups. (A) Stacked bar chart showing the overall composition of major immune cell categories (myeloid cells, T cells, NK cells, and B cells) in the HD and PA groups. Data represent mean proportions of $CD45^{+}$ cells. (B) Box plots comparing the proportions of key immune cell populations between the HD and PA groups. Each dot represents an individual sample. (C) Forest plot displaying Cohen's d effect sizes with 95% confidence intervals for each cell population comparison. The dashed vertical line indicates zero (no effect). Effect sizes are classified as large (|d| ≥ 0.8), medium (0.5 ≤ |d| < 0.8), small (0.2 ≤ |d| < 0.5), or negligible (|d| < 0.2). HD, n = 6; PA, n = 14. Green, HD group; red, PA group. HD, healthy donors; PA, HBV-infected pregnant women; CI, confidence interval.

Marker expression changes in NK cell subsets

The two major NK cell subsets showed nominal upregulation of activation- and cytotoxicity-related markers in the PA group (raw $P < 0.05$; none survived FDR < 0.1 correction) (Supplementary Fig. 2B and C).

In $CD38^{hi}$ $CD56^{dim}$ $CD16^{+}$ NK cells (Cluster 1), CD38 expression tended to be upregulated (raw $P = 0.0044$, FC = 1.33; FDR > 0.1) (Supplementary Fig. 3A). CD16 (raw $P = 0.023$, FC = 1.13), CD123 (raw $P = 0.0074$, FC = 1.27), and CD31 (raw $P = 0.0094$, FC = 1.13) were also nominally upregulated, while αSMA showed nominal downregulation (raw $P = 0.0057$, FC = 0.86).

In $CD56^{dim}$ $CD16^{+}$ $CD57^{+}$ mature NK cells (Cluster 3), CD16 was nominally upregulated (raw $P = 0.0020$, FC = 1.30) (Supplementary Fig. 3B). CD11c (raw $P = 0.0094$, FC = 1.25), CD38 (raw $P = 0.015$, FC = 1.45), and CD31 (raw $P = 0.043$, FC = 1.13) were similarly nominally upregulated.

Correlation analysis between CD38 and CD16 (Fig. 4A and B; Table 4) revealed that in mature NK cells (Cluster 3), CD38 and CD16 showed a strong positive correlation (all samples: $\rho = 0.872$, $P < 0.0001$), with $\rho = 0.886$ ($P = 0.033$) in the HD group and $\rho = 0.732$ ($P = 0.004$) in the PA group. In $CD38^{hi}$ NK cells (Cluster 1), the correlations were as follows: all samples, $\rho = 0.675$ ($P = 0.0015$); HD group, $\rho = 1.0$ ($P = 0.003$); and PA group, $\rho = 0.332$ ($P = 0.246$).

Marker expression changes in T cell subsets

Multiple T cell subsets showed nominal upregulation of activation- and migration-related markers in the PA group (raw $P < 0.05$; none survived FDR correction) (Supplementary Fig. 4A–C).

In naive CD4 T cells (Cluster 4), CD27 was nominally upregulated (raw $P = 0.0057$, FC = 1.31), accompanied by nominal upregulation of CD38 (raw $P = 0.019$, FC = 1.49) and CD185 (raw $P = 0.043$, FC = 1.13). CD185 was nominally upregulated across multiple cell subsets, including activated late-differentiated CD8 T cells (Cluster 2, raw $P = 0.019$), naive CD8 T cells (Cluster 5, raw $P = 0.035$), activated CD4 effector memory-like T cells (Cluster 6, raw $P = 0.035$), and $CD56^{bright}$ NK cells (Cluster 7, raw $P = 0.012$).

Correlation analysis between CD27 and CD185 (Fig. 4C–E) showed the following: Cluster 4, all samples, $\rho = 0.430$ ($P = 0.060$); Cluster 5, all samples, $\rho = 0.415$ ($P = 0.070$); and Cluster 6, all samples, $\rho = 0.450$ ($P = 0.048$).

Marker expression changes in basophils

Basophils (Cluster 11) displayed nine candidate differential markers in the PA group with nominal significance (all raw $P < 0.05$, uncorrected; none survived FDR < 0.1), all showing a downregulation trend (Supplementary Fig. 4D). The nominally downregulated markers included CD194/CCR4 (raw $P = 0.012$, FC = 0.49), CD183/CXCR3 (raw $P = 0.029$, FC = 0.81), CD185/CXCR5 (raw $P = 0.029$, FC = 0.73), CD197/CCR7 (raw $P = 0.043$, FC = 0.73), CD45RA (raw $P = 0.0057$, FC = 0.63), CD105 (raw $P = 0.0094$, FC = 0.73), CD56 (raw $P = 0.029$, FC = 0.77), CD3 (raw $P = 0.043$, FC = 0.85), and αSMA (raw $P = 0.019$, FC = 0.67) (Supplementary Fig. 3C and D).

Correlation analysis between CD194 and CD197 (Fig. 4F) revealed the following: all samples, $\rho = 0.571$ ($P = 0.010$); HD group, $\rho = 0.886$ ($P = 0.033$); and PA group, $\rho = 0.116$ ($P = 0.693$).

Marker expression changes in monocytes

Classical monocytes (Cluster 12) showed six candidate differential markers with nominal significance (raw $P < 0.05$; 1↑/5↓; none survived FDR correction) (Supplementary Fig. 4E). CD38 was nominally upregulated (raw $P = 0.012$, FC = 1.41), while CD163 was nominally downregulated (raw $P = 0.029$, FC = 0.78) (Supplementary Fig. 3E and F). Other nominally downregulated markers included CD24 (raw $P = 0.019$), CD3 (raw $P = 0.023$, FC = 0.44), αSMA (raw $P = 0.029$), and CD8 (raw $P = 0.043$).

Intermediate monocytes (Cluster 13) showed four candidate differential markers with nominal significance (raw $P < 0.05$; 3↑/1↓) (Supplementary Fig. 4F): CD185 (raw $P = 0.0074$, FC = 1.07), CD38 (raw $P = 0.035$, FC = 1.48), and CD11B (raw $P = 0.043$, FC = 1.04) were nominally upregulated, while CD3 was nominally downregulated (raw $P = 0.0057$, FC = 0.39).

Correlation analysis between CD38 and CD163 (Fig. 4G) showed the following: all samples, $\rho = -0.194$ ($P = 0.411$); HD group, $\rho = 0.657$ ($P = 0.175$); and PA group, $\rho = -0.02$ ($P = 0.952$).

Consistent changes across cell subsets and summary of correlation analyses

CD38 showed a consistent nominal upregulation trend across five different cell subsets (raw $P < 0.05$; none survived FDR correction): Cluster 1 (raw $P = 0.0044$, FC = 1.33), Cluster 3 (raw $P = 0.015$, FC = 1.45), Cluster 4 (raw $P = 0.019$, FC = 1.49), Cluster 12 (raw $P = 0.012$, FC = 1.41), and Cluster 13 (raw $P = 0.035$, FC = 1.48) (Fig. 4H).

CD16 was nominally upregulated in two NK cell subsets: Cluster 1 (raw $P = 0.023$, FC = 1.13) and Cluster 3 (raw $P = 0.002$, FC = 1.30) (Fig. 4I).

CD3 showed a nominal downregulation trend across multiple myeloid cell subsets: Cluster 9 (raw $P = 0.043$), Cluster 10 (raw $P = 0.029$), Cluster 11 (raw $P = 0.043$), Cluster 12 (raw $P = 0.023$), and Cluster 13 (raw $P = 0.0057$) (Supplementary Fig. 3G).

Correlation analyses evaluated seven key marker pairs (Table 4; Fig. 4A–G). The CD38–CD16 correlation in NK cells was the strongest (Cluster 3: $\rho = 0.872$, $P < 0.001$). In $CD38^{hi}$ NK cells and basophils, strong correlations observed in the HD group were attenuated in the PA group: the Cluster 1 CD38–CD16 correlation decreased from $\rho = 1.0$ in the HD group to $\rho = 0.332$ in the PA group; the Cluster 11 CD194–CD197 correlation decreased from $\rho = 0.886$ in the HD group to $\rho = 0.116$ in the PA group.

Exploratory stratified analysis by viral load

To examine whether the immune changes in the PA group were related to viral activity, we divided the PA group according to HBV DNA levels ($\geq 10^3$ IU/mL, n = 6 vs. $<10^3$ IU/mL, n = 8). In our cohort, this grouping was identical to HBeAg-positive versus HBeAg-negative status, and all high viral load cases had received TDF antiviral treatment.

At the cell subset level, Mann–Whitney U tests showed no significant differences in any of the 13 immune cell subsets between the two subgroups (all raw $P > 0.05$; Supplementary Table 6). Five cell subsets showed medium or large effect sizes (|Cohen's d| ≥ 0.5): $CD38^{hi}$ $CD56^{dim}$ $CD16^{+}$ NK cells (d = −0.94, raw $P = 0.081$, FC = 0.68), naive CD4 T cells (d = −0.73, FC = 0.80), $CD56^{bright}$ NK cells (d = 0.60, FC = 1.88), B cells (d = −0.60, FC = 0.75), and $CD56^{dim}$ $CD16^{+}$ $CD57^{+}$ mature NK cells (d = 0.51, FC = 1.41).

At the marker expression level, we further compared 35 functional markers across the 13 cell subsets (455 comparisons in total). Only seven comparisons (1.5%) reached raw $P < 0.05$, lower than the 5% expected by chance, and none remained significant after FDR correction (Supplementary Table 7).

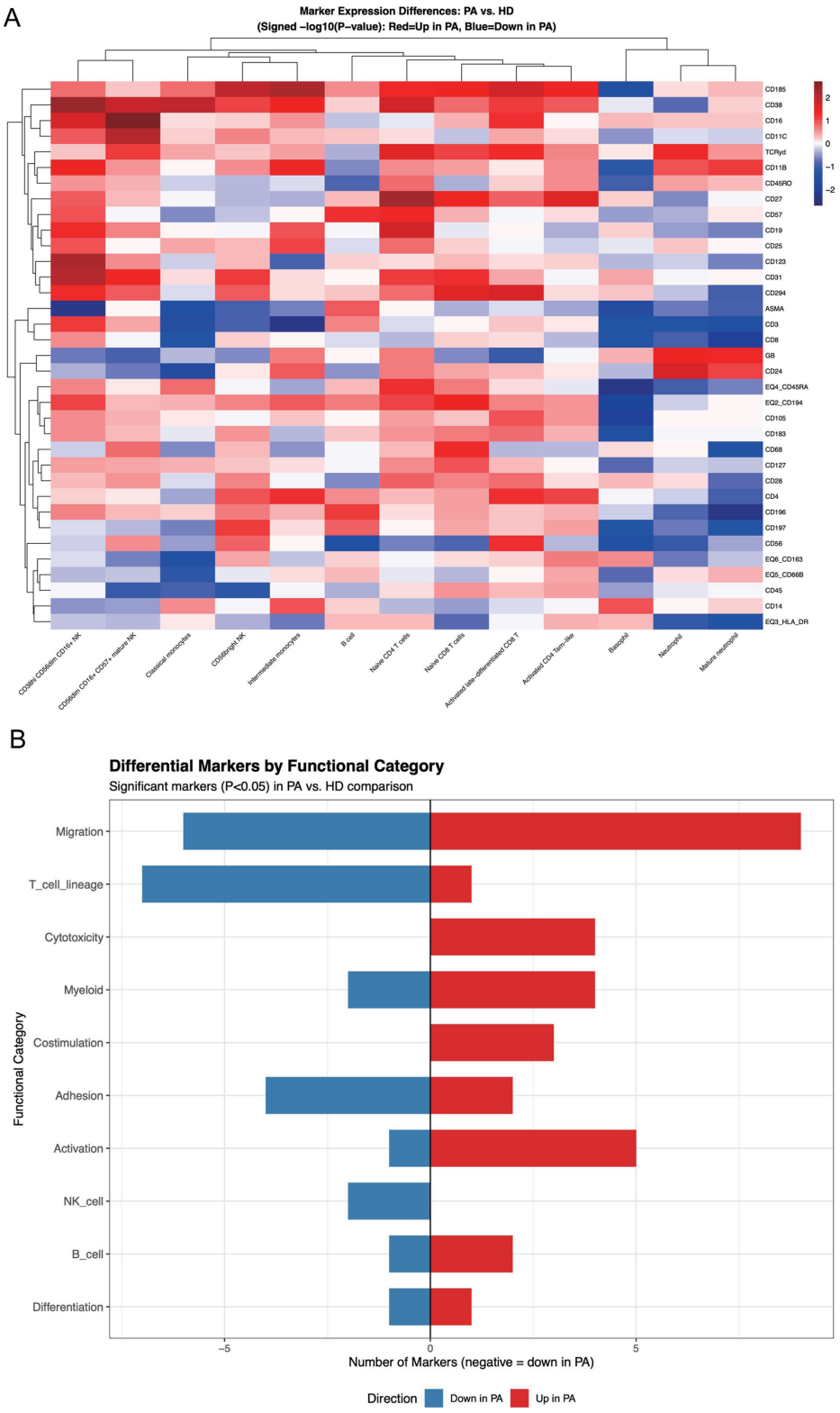

Fig. 3. Overview of differential marker expression across immune cell clusters. (A) Heatmap showing signed −log10(*P*-value) for marker expression differences between the PA and HD groups across 13 immune cell clusters. Red indicates upregulation in the PA group; blue indicates downregulation. Color intensity reflects statistical significance. Rows represent markers (n = 35); columns represent cell clusters. (B) Bar plot summarizing the number of differentially expressed markers ($P < 0.05$) by functional category. Red bars indicate markers upregulated in the PA group; blue bars indicate markers downregulated. Functional categories are ordered by the total number of differential markers. HD, n = 6; PA, n = 14. HD, healthy donors; PA, HBV-infected pregnant women.

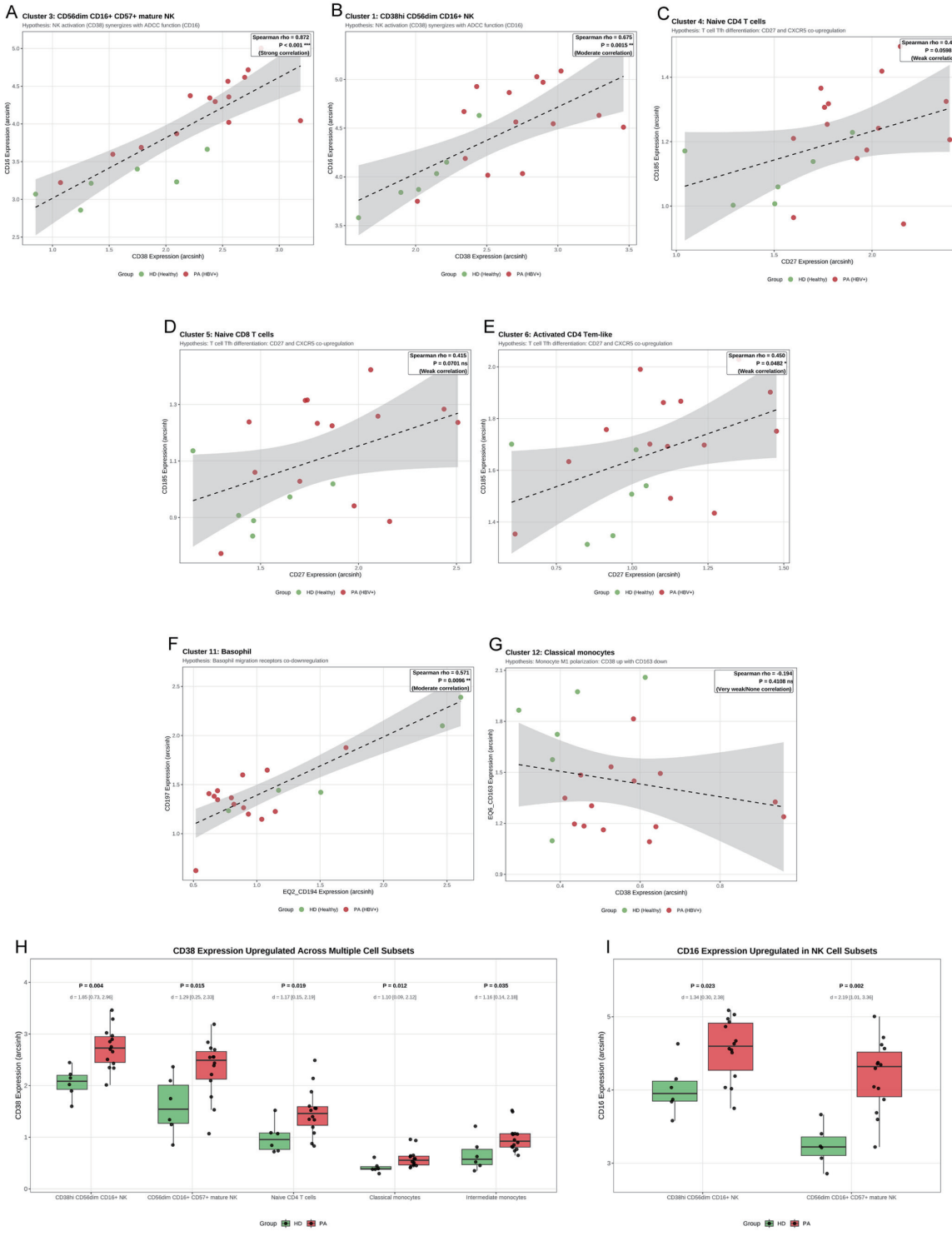

Fig. 4. Correlation analyses and cross-cluster marker expression patterns. (A–B) Correlation between CD38 and CD16 expression in NK cell subsets. (A) $CD38^{hi}$ $CD56^{dim}$ $CD16^{+}$ NK cells (Cluster 1). (B) $CD56^{dim}$ $CD16^{+}$ $CD57^{+}$ mature NK cells (Cluster 3). (C–E) Correlation between CD27 and CD185 (CXCR5) expression in T-cell subsets. (C) Naive CD4 T cells (Cluster 4). (D) Naive CD8 T cells (Cluster 5). (E) Activated CD4 Tem-like cells (Cluster 6). (F) Correlation between CD194 (CCR4) and CD197 (CCR7) expression in basophils (Cluster 11). (G) Correlation between CD38 and CD163 expression in classical monocytes (Cluster 12). (H) Box plots showing CD38 expression across five cell clusters with upregulation in the PA group: $CD38^{hi}$ $CD56^{dim}$ $CD16^{+}$ NK (Cluster 1), $CD56^{dim}$ $CD16^{+}$ $CD57^{+}$ mature NK (Cluster 3), naive CD4 T cells (Cluster 4), classical monocytes (Cluster 12), and intermediate monocytes (Cluster 13). Statistical comparisons are shown for each cluster. (I) Box plots showing CD16 expression in two NK cell subsets with upregulation in the PA group: $CD38^{hi}$ $CD56^{dim}$ $CD16^{+}$ NK (Cluster 1) and $CD56^{dim}$ $CD16^{+}$ $CD57^{+}$ mature NK (Cluster 3). HD, n = 6; PA, n = 14. Green, HD group; red, PA group. HD, healthy donors; PA, HBV-infected pregnant women; NK, natural killer cells; Tem, effector memory T cells; CXCR5, C-X-C chemokine receptor type 5; CCR4, C-C chemokine receptor type 4; CCR7, C-C chemokine receptor type 7; CI, confidence interval.

Table 4. Spearman correlation analysis of key marker pairs across immune cell subsets

Cluster	Cell population	Marker1	Marker2	ρ (All)	*P* (All)	ρ (HD)	*P* (HD)	ρ (PA)	*P* (PA)	Hypothesis	Expected	Analysis	Supports
1	$CD38^{hi}$ $CD56^{dim}$ $CD16^{+}$ NK	CD38	CD16	0.675	0.0015	1.000	0.0028	0.332	0.2463	NK activation (CD38) synergizes with ADCC function (CD16)	positive	NK Activation ADCC	Yes
3	$CD56^{dim}$ $CD16^{+}$ $CD57^{+}$ mature NK	CD38	CD16	0.872	<0.0001	0.886	0.0333	0.732	0.0041	NK activation (CD38) synergizes with ADCC function (CD16)	positive	NK Activation ADCC	Yes
12	Classical monocytes	CD38	EQ6_ CD163	−0.194	0.4108	0.657	0.1750	−0.020	0.9517	Monocyte M1 polarization: CD38 up with CD163 down	negative	Monocyte M1M2 Polarization	No/ Uncertain
4	Naive CD4 T cells	CD27	CD185	0.430	0.0598	0.429	0.4194	0.086	0.7732	T cell Tfh differentiation: CD27 and CXCR5 co-upregulation	positive	Tcell Tfh Differentiation	No/ Uncertain
5	Naive CD8 T cells	CD27	CD185	0.415	0.0701	−0.029	1.0000	0.235	0.4175	T cell Tfh differentiation: CD27 and CXCR5 co-upregulation	positive	Tcell Tfh Differentiation	No/ Uncertain
6	Activated CD4 Tem-like	CD27	CD185	0.450	0.0482	0.086	0.9194	0.314	0.2735	T cell Tfh differentiation: CD27 and CXCR5 co-upregulation	positive	Tcell Tfh Differentiation	Yes
11	Basophil	EQ2_ CD194	CD197	0.571	0.0096	0.886	0.0333	0.116	0.6930	Basophil migration receptors co-downregulation	positive	Basophil Migration	Yes

Rho, Spearman correlation coefficient; HD, healthy donors; PA, HBV-infected pregnant women; NK, natural killer cells; ADCC, antibody-dependent cellular cytotoxicity; Tfh, follicular helper T cells; Tem, effector memory T cells. Statistical analysis: Spearman rank correlation was used for all analyses. Correlations were calculated for all samples combined (All, n = 20), the HD group (n = 6), and the PA group (n = 14) separately. Hypothesis testing: "Supports" was determined as "Yes" if the correlation direction matched the expected direction and $P < 0.05$ in the combined analysis; "No/Uncertain" indicates either an opposite direction or a nonsignificant correlation.

Discussion

This study used mass cytometry to characterize the impact of chronic HBV infection on placental immune cell composition, functional marker expression, and expression coordination. Our exploratory findings suggest that HBV infection may induce cell type-specific functional remodeling rather than changes in immune cell composition: NK cells and T cells tended to show enhanced activation, basophils showed a trend of extensive functional downregulation, and the expression coordination between multiple marker pairs appeared to be weakened across cell subsets. It should be emphasized that these between-group differences were based on raw *P*-values, and none survived FDR < 0.1 correction; therefore, these findings should be regarded as hypothesis-generating signals warranting validation in larger cohorts.

In our study, both CD38 and CD16 were nominally upregulated (raw $P < 0.05$, uncorrected) in the NK cell subsets, and the two markers showed a strong positive correlation in mature NK cells (based on Spearman analysis of raw expression values). The upregulation of CD38 is consistent with previous reports on the activation of NK cells in chronic HBV infection.[47] Interestingly, although some studies reported that peripheral blood CD16 was downregulated in chronic HBV infection,[48] we observed a significant upregulation of CD16 in the placenta. The coordinated upregulation of CD38 and CD16, together with their strong positive correlation, suggests a unique and tissue-specific ADCC functional synergy in the placental microenvironment. The coordinated expression of CD38 and CD16 has been shown to enhance ADCC function,[14,49] and our correlation analysis provides supporting evidence for this functional synergy. It is worth noting that the response of $CD56^{dim}$ $CD16^{+}$ NK cells to HBV infection is more pronounced than that of the $CD56^{bright}$ subset. Although decidual NK cells are mainly of the $CD56^{bright}$ phenotype and are primarily involved in vascular remodeling and the maintenance of immune tolerance,[6,50] our results suggest that the $CD56^{dim}$ subset may play a more critical role in the antiviral response. This selective activation pattern may represent a finely regulated immune strategy: retaining pregnancy immune tolerance while selectively enhancing the ADCC-competent subset to counter the viral threat.

Enhanced NK cell activation and ADCC function may form an immune barrier in the placenta against the vertical transmission of HBV. Considering that the vast majority of pregnant women infected with HBV—especially those who have received immunoprophylaxis—do not transmit the virus to their offspring, this compensatory immune activation may be one of the mechanisms that block viral transmission. However, this hypothesis needs to be verified by comparing the immune phenotypes of transmitting and non-transmitting cases.

The most unexpected finding in this study is the extensive functional downregulation trend of basophils. All 9 candidate markers with nominal significance (raw $P < 0.05$, uncorrected) showed a consistent downward trend, covering a variety of chemokine receptors, differentiation markers, and adhesion molecules. Although none of these markers survived FDR < 0.1 correction, the consistent directional pattern across functionally related markers suggests that this finding may carry biological meaning warranting further investigation.

Basophils have been well established as producers of Th2 cytokines (including IL-4 and IL-13) involved in allergic and inflammatory reactions.[11,16] Considering that the maintenance of normal pregnancy depends on a Th2-dominant immune environment,[12] we speculate that the extensive functional downregulation observed in this study may compromise the availability of Th2 cytokines at the maternal–fetal interface, which may affect placental immune homeostasis. Regarding the potential mechanisms, we speculate that continuous antigen stimulation during chronic viral infection may induce functional exhaustion[51]; functionally competent basophils may selectively migrate to peripheral blood or other tissues; and HBV infection may impair the differentiation and maturation of basophils.

What is particularly interesting is that the expression coordination between CCR4 and CCR7 in the PA group was markedly weakened compared with that in the HD group. CCR4 and CCR7 mediate migration toward the placenta and secondary lymphoid organs, respectively,[52–54] and this loss of coordination suggests that HBV infection may disrupt the migratory regulatory network of basophils.

From a clinical perspective, our study provides the preliminary evidence that basophil markers in HBV-infected placentas are widely downregulated. Considering their ability to produce Th2 cytokines in allergic and inflammatory contexts,[11,16] the functional impairment of basophils may significantly disrupt placental immune homeostasis. The consistent downregulation pattern across multiple markers highlights their potential as biomarkers of placental immune status during HBV infection. However, since our analysis is limited to surface markers, functional assays are needed in the future to determine whether the cytokine secretion capacity of basophils is truly impaired, and these phenotypic characteristics must also be verified in prospective cohorts with documented MTCT outcomes.

Classical monocytes showed CD38 upregulation accompanied by CD163 downregulation, which is consistent with the M1 polarization trajectory and in line with previous reports on monocyte M1 polarization during chronic viral infection.[55] However, the expected negative correlation between CD38 and CD163 did not reach statistical significance. This may be attributed to the following factors: limited sample size and insufficient statistical power; placental monocytes may show a "hybrid phenotype" and simultaneously express M1 and M2 markers[56]; and CD38 and CD163 may be regulated by independent signaling pathways. Although the correlation was not significant, the independent changes of CD38 upregulation and CD163 downregulation still suggest that monocyte activation is enhanced, which may promote antiviral responses but may also foster a proinflammatory environment.

In addition to the cell type-specific findings, this study also reveals a cross-subset pattern: HBV infection leads to a weakening of expression coordination between multiple functional marker pairs. In $CD38^{hi}$ $CD56^{dim}$ $CD16^{+}$ NK cells, the strong CD38–CD16 correlation observed in the HD group was markedly weakened in the PA group; similarly, in basophils, the CCR4–CCR7 correlation was also markedly weakened. This loss of coordination may reflect the disruption of intracellular signal transduction networks by HBV infection,[57] suggesting that the impact of the virus is not only limited to changes in marker expression levels but also involves more fundamental changes in the regulatory relationships between markers.

Our exploratory stratified analysis within the PA group by viral load (HBV DNA $\geq 10^3$ vs. $<10^3$ IU/mL) did not reveal significant differences in any immune cell subset or marker expression, although $CD38^{hi}$ $CD56^{dim}$ $CD16^{+}$ NK cells and naive CD4 T cells showed medium-to-large effect sizes and were lower in the high viral load subgroup. This suggests that the immune changes observed in the PA group are not driven solely by high viral load and may reflect a broader response to chronic HBV infection.

Although our findings are exploratory and need to be confirmed in larger studies, they have several implications for the clinical management of HBV in pregnancy.

First, under the current standard of care, that is, com-

bined immunoprophylaxis (hepatitis B immunoglobulin plus vaccine), together with maternal tenofovir for those with a high viral load, MTCT still occurs in about 5–10% of high-risk pregnancies. Our data suggest that the placenta is not just a passive barrier but an active immune site that can be altered by chronic HBV infection, especially in NK cells and basophils. This suggests that the remaining MTCT risk cannot be explained solely by maternal viral load, and the immune status of the placenta may also need to be considered in clinical risk assessment.

Second, the changes in NK cells and basophils found in this study may serve as candidate placental markers for risk stratification. If confirmed in larger studies with clear transmission outcomes, these markers could help identify pregnancies in which standard immunoprophylaxis may be insufficient, allowing closer follow-up or adjusted antiviral treatment to be considered.

Third, because placental tissue can only be obtained after delivery, it cannot be used for real-time clinical decision-making during pregnancy. However, our results support future studies to test whether basophils and NK cells in maternal peripheral blood can reflect the immune status of the placenta. If such blood-based markers can be established, the maternal–fetal immune environment could be monitored during pregnancy without invasive sampling.

Fourth, the reduced basophil activation and the shift in NK cell subsets suggest that, in addition to viral suppression, local immune regulation may also help prevent MTCT. This provides a biological basis for exploring additional immunomodulatory treatments in patients who remain at risk despite receiving optimal antiviral therapy. It also supports individualized decision-making regarding when to initiate tenofovir treatment and how long to continue it, based on both virological and immunological indicators.

Finally, we emphasize that these translational implications should be regarded as hypotheses rather than conclusions. Before these findings can be applied in clinical practice, prospective studies are needed to link placental immune profiles with actual transmission outcomes and peripheral immune markers.

This study has some limitations. First, the small sample size (n = 20) limits statistical power, and no marker reached significance after FDR correction. Therefore, all between-group differences reported in this study are based on raw *P*-values and should be viewed as nominal signals rather than confirmed differences. Even so, the consistent direction of changes observed across cell subsets and the effect size results suggest that these findings warrant testing in future studies. Second, the cross-sectional design at term delivery cannot capture dynamic immune changes throughout pregnancy. Third, mass cytometry can only detect surface markers, and functional validation—including ADCC activity and cytokine secretion—has yet to be carried out. Fourth, although we performed exploratory stratified analyses at both the cell subset and marker expression levels, $HBeAg^+$ status and high HBV DNA load ($\geq 10^3$ IU/mL) were completely overlapping in our cohort, and TDF treatment substantially overlapped with both (all 6 $HBeAg^+$ patients and 4 of 8 HBeAg− patients received TDF); therefore, we cannot separate the effects of viral activity itself from those of antiviral therapy. Larger studies spanning a wider range of viral loads and including patients with different timings of antiviral therapy initiation are needed to clarify these relationships. Fifth, this study did not link placental immune alterations to MTCT outcomes or HBV-specific T-cell responses in neonates, as MTCT follow-up requires serological testing at 7–12 months of age and the original ethical approval did not cover neonatal blood sampling. Sixth, the enzymatic digestion used in tissue processing may cleave some surface epitopes, such as chemokine receptors and adhesion molecules. As all samples were processed identically, between-group comparisons should remain reliable; however, the absolute expression levels of these markers may be lower than their true in situ levels and should be interpreted with this in mind. Seventh, anti-HBs status was not routinely measured in the HD group, as our clinical screening protocol only required HBsAg negativity to exclude HBV infection. Although anti-HBs positivity, reflecting prior vaccination or resolved infection, is generally not associated with substantial alterations in the placental immune microenvironment, the lack of these data prevents us from formally excluding a residual influence of prior HBV exposure on the control profiles. Future studies should prospectively collect anti-HBs serology to further validate our findings. We position this work as an exploratory study designed to generate hypotheses and identify candidate markers for subsequent functional validation in larger-scale longitudinal cohorts.

Conclusions

In summary, this study reveals that HBV infection induces functional remodeling rather than compositional changes in placental immune cells. NK cells and T cells showed upregulation of activation and cytotoxicity markers, suggesting enhanced ADCC function; however, basophils showed extensive downregulation of migration-related markers and loss of expression coordination—an unprecedented finding. The weakening of coordination between multiple marker pairs suggests that HBV infection has disrupted the immune regulatory network.

To our knowledge, this study is the first to apply high-dimensional single-cell technology to comprehensively characterize the immune-cell landscape in sampled placental tissue, identify the novel phenomenon of basophil functional downregulation, and introduce marker coordination analysis as a methodological approach. These findings provide new insights into the immunological mechanisms underlying HBV MTCT.

Future studies should prioritize functional validation of basophil changes (IL-4/IL-13 secretion) and their association with transmission outcomes, as well as verification in larger-scale longitudinal cohorts. In particular, a prospective cohort with documented MTCT outcomes and paired neonatal blood samples is needed to determine whether the placental immune signatures identified here correlate with HBV-specific T-cell responses in neonates. The candidate markers identified in this study provide a basis for subsequent mechanistic research and clinical translation.

Supporting information

Supplementary material for this article is available at https://doi.org/10.14218/JCTH.2026.00429.

Funding

This work was supported by the Beijing Natural Science Foundation ([7232080] to JL) and the Fengtai District Health System Scientific Research Project ([2023-66] to YZ).

Conflict of interest

The authors have no conflict of interests related to this publication.

Author contributions

Study concept and design (WW, JL, YZ), acquisition of data (ZY, LQ, WZ), analysis and interpretation of data (ZY, LQ), drafting of the manuscript (ZY, LQ), critical revision of the manuscript for important intellectual content (WW, JL), statistical analysis (ZY, LQ, YB), funding acquisition (JL, YZ), administrative, technical, or material support (WW, JL), and study supervision (WW, JL, YZ). All authors made significant contributions to this study and approved the final manuscript.

Ethical statement

This study was approved by the Ethics Committee of Beijing You An Hospital, Capital Medical University (Approval No. LL-2024-001-K). Written informed consent was obtained from all participants prior to sample collection. The study was conducted in accordance with the principles of the Declaration of Helsinki (as revised in 2024).

Data sharing statement

The mass cytometry dataset and statistical code used to support the findings of this study are available from the corresponding authors at junfengdoc@ccmu.edu.cn (JL) and zyx0718@ccmu.edu.cn (YZ) upon reasonable request.

References

[1] Shen F, Li B, Lv H, Li Z, Li D, Yang H, *et al*. Global, regional, and national burden of chronic hepatitis B, 1990-2021, and projections to 2030: An urgent call for action to achieve hepatitis B elimination goals by 2030. Hum Vaccin Immunother 2026;22(1):2641857. doi:10.1080/21645515.2026.2641857, PMID:41804590.

[2] Yan R, Sun M, Yang H, Du S, Sun L, Mao Y. 2024 latest report on hepatitis B virus epidemiology in China: current status, changing trajectory, and challenges. Hepatobiliary Surg Nutr 2025;14(1):66–77. doi:10.21037/hbsn-2024-754, PMID:39925891.

[3] Liu JF, Chen TY, Zhao YR. Vertical transmission of hepatitis B virus: propositions and future directions. Chin Med J (Engl) 2021;134(23):2825–2831. doi:10.1097/CM9.0000000000001800, PMID:34636774.

[4] Motomura K, Hara M, Ito I, Morita H, Matsumoto K. Roles of human trophoblasts' pattern recognition receptors in host defense and pregnancy complications. J Reprod Immunol 2023;156:103811. doi:10.1016/j.jri.2023.103811, PMID:36669386.

[5] Megli CJ, Coyne CB. Infections at the maternal-fetal interface: an overview of pathogenesis and defence. Nat Rev Microbiol 2022;20(2):67–82. doi:10.1038/s41579-021-00610-y, PMID:34433930.

[6] Zhang X, Wei H. Role of Decidual Natural Killer Cells in Human Pregnancy and Related Pregnancy Complications. Front Immunol 2021;12:728291. doi:10.3389/fimmu.2021.728291, PMID:34512661.

[7] Menzies FM. The Placenta as an Immunological Environment. Br J Biomed Sci 2025;82:14910. doi:10.3389/bjbs.2025.14910, PMID:41341663.

[8] Feyaerts D, Benner M, Comitini G, Shadmanfar W, van der Heijden OWH, Joosten I, *et al*. NK cell receptor profiling of endometrial and decidual NK cells reveals pregnancy-induced adaptations. Front Immunol 2024;15:1353556. doi:10.3389/fimmu.2024.1353556, PMID:38571943.

[9] Guan D, Chen Z, Zhang Y, Sun W, Li L, Huang X. Dual Role of Natural Killer Cells in Early Pregnancy: Immunopathological Implications and Therapeutic Potential in Recurrent Spontaneous Abortion and Recurrent Implantation Failure. Cell Prolif 2025;58(9):e70037. doi:10.1111/cpr.70037, PMID:40325291.

[10] Girsch JH, Mejia Plazas MC, Olivier A, Farah M, Littlefield D, Behl S, *et al*. Host-Viral Interactions at the Maternal-Fetal Interface. What We Know and What We Need to Know. Frontiers (Boulder) 2022;2:833106. doi:10.3389/fviro.2022.833106, PMID:36742289.

[11] Iype J, Fux M. Basophils Orchestrating Eosinophils' Chemotaxis and Function in Allergic Inflammation. Cells 2021;10(4):895. doi:10.3390/cells10040895, PMID:33919759.

[12] Chatterjee P, Chiasson VL, Bounds KR, Mitchell BM. Regulation of the Anti-Inflammatory Cytokines Interleukin-4 and Interleukin-10 during Pregnancy. Front Immunol 2014;5:253. doi:10.3389/fimmu.2014.00253, PMID:24904596.

[13] Morandi F, Airoldi I, Marimpietri D, Bracci C, Faini AC, Gramignoli R. CD38, a Receptor with Multifunctional Activities: From Modulatory Functions on Regulatory Cell Subsets and Extracellular Vesicles, to a Target for Therapeutic Strategies. Cells 2019;8(12):1527. doi:10.3390/cells8121527, PMID:31783629.

[14] Zambello R, Barilà G, Manni S, Piazza F, Semenzato G. NK cells and CD38: Implication for (Immuno)Therapy in Plasma Cell Dyscrasias. Cells 2020;9(3):768. doi:10.3390/cells9030768, PMID:32245149.

[15] Ni D, Zhou H, Wang P, Xu F, Li C. Visualizing Macrophage Phenotypes and Polarization in Diseases: From Biomarkers to Molecular Probes. Phenomics 2023;3(6):613–638. doi:10.1007/s43657-023-00129-7, PMID:38223685.

[16] Min B, Paul WE. Basophils and type 2 immunity. Curr Opin Hematol 2008;15(1):59–63. doi:10.1097/MOH.0b013e3282f13ce8, PMID:18043247.

[17] Gao F, Wang H, Li X, Guo F, Yuan Y, Wang X, *et al*. Alteration of the Immune Microenvironment in HBsAg and HBeAg Dual-Positive Pregnant Women Presenting a High HBV Viral Load. J Inflamm Res 2021;14:5619–5632. doi:10.2147/JIR.S337561, PMID:34764667.

[18] Lin Y, Liu Y, Xu D, Guo F, Zhang W, Zhang Y, *et al*. HBxAg promotes HBV replication and EGFR activation in human placental trophoblasts. Exp Ther Med 2021;22(5):1211. doi:10.3892/etm.2021.10645, PMID:34584556.

[19] Spitzer MH, Nolan GP. Mass Cytometry: Single Cells, Many Features. Cell 2016;165(4):780–791. doi:10.1016/j.cell.2016.04.019, PMID:27153492.

[20] Ornatsky O, Bandura D, Baranov V, Nitz M, Winnik MA, Tanner S. Highly multiparametric analysis by mass cytometry. J Immunol Methods 2010;361(1-2):1–20. doi:10.1016/j.jim.2010.07.002, PMID:20655312.

[21] von Elm E, Altman DG, Egger M, Pocock SJ, Gøtzsche PC, Vandenbroucke JP, *et al*. The Strengthening the Reporting of Observational Studies in Epidemiology (STROBE) statement: guidelines for reporting observational studies. J Clin Epidemiol 2008;61(4):344–349. doi:10.1016/j.jclinepi.2007.11.008, PMID:18313558.

[22] World Medical Association. World Medical Association Declaration of Helsinki: ethical principles for medical research involving human subjects. JAMA 2013;310(20):2191–2194. doi:10.1001/jama.2013.281053, PMID:24141714.

[23] European Association for the Study of the Liver. EASL 2017 Clinical Practice Guidelines on the management of hepatitis B virus infection. J Hepatol 2017;67(2):370–398. doi:10.1016/j.jhep.2017.03.021, PMID:28427875.

[24] Burton GJ, Sebire NJ, Myatt L, Tannetta D, Wang YL, Sadovsky Y, *et al*. Optimising sample collection for placental research. Placenta 2014;35(1):9–22. doi:10.1016/j.placenta.2013.11.005, PMID:24290528.

[25] Aplin JD, Myers JE, Timms K, Westwood M. Tracking placental development in health and disease. Nat Rev Endocrinol 2020;16(9):479–494. doi:10.1038/s41574-020-0372-6, PMID:32601352.

[26] Reichard A, Asosingh K. Best Practices for Preparing a Single Cell Suspension from Solid Tissues for Flow Cytometry. Cytometry A 2019;95(2):219–226. doi:10.1002/cyto.a.23690, PMID:30523671.

[27] Leelatian N, Doxie DB, Greenplate AR, Mobley BC, Lehman JM, Sinnaeve J, *et al*. Single cell analysis of human tissues and solid tumors with mass cytometry. Cytometry B Clin Cytom 2017;92(1):68–78. doi:10.1002/cyto.b.21481, PMID:27598832.

[28] Stacey GN, Masters JR. Cryopreservation and banking of mammalian cell lines. Nat Protoc 2008;3(12):1981–1989. doi:10.1038/nprot.2008.190, PMID:19180080.

[29] Fienberg HG, Simonds EF, Fantl WJ, Nolan GP, Bodenmiller B. A platinum-based covalent viability reagent for single-cell mass cytometry. Cytometry A 2012;81(6):467–475. doi:10.1002/cyto.a.22067, PMID:22577098.

[30] Han G, Spitzer MH, Bendall SC, Fantl WJ, Nolan GP. Metal-isotope-tagged monoclonal antibodies for high-dimensional mass cytometry. Nat Protoc 2018;13(10):2121–2148. doi:10.1038/s41596-018-0016-7, PMID:30258176.

[31] Getz EB, Xiao M, Chakrabarty T, Cooke R, Selvin PR. A comparison between the sulfhydryl reductants tris(2-carboxyethyl)phosphine and dithiothreitol for use in protein biochemistry. Anal Biochem 1999;273(1):73–80. doi:10.1006/abio.1999.4203, PMID:10452801.

[32] Chevrier S, Crowell HL, Zanotelli VRT, Engler S, Robinson MD, Bodenmiller B. Compensation of Signal Spillover in Suspension and Imaging Mass Cytometry. Cell Syst 2018;6(5):612–620.e5. doi:10.1016/j.cels.2018.02.010, PMID:29605184.

[33] Bendall SC, Simonds EF, Qiu P, Amir el-AD, Krutzik PO, Finck R, *et al*. Single-cell mass cytometry of differential immune and drug responses across a human hematopoietic continuum. Science 2011;332(6030):687–696. doi:10.1126/science.1198704, PMID:21551058.

[34] Maecker HT, McCoy JP, Nussenblatt R. Standardizing immunophenotyping for the Human Immunology Project. Nat Rev Immunol 2012;12(3):191–200. doi:10.1038/nri3158, PMID:22343568.

[35] Zunder ER, Finck R, Behbehani GK, Amir el-AD, Krishnaswamy S, Gonzalez VD, *et al*. Palladium-based mass tag cell barcoding with a doublet-filtering scheme and single-cell deconvolution algorithm. Nat Protoc 2015;10(2):316–333. doi:10.1038/nprot.2015.020, PMID:25612231.

[36] Iyer A, Hamers AAJ, Pillai AB. CyTOF(®) for the Masses. Front Immunol 2022;13:815828. doi:10.3389/fimmu.2022.815828, PMID:35493491.

[37] Finck R, Simonds EF, Jager A, Krishnaswamy S, Sachs K, Fantl W, *et al*. Normalization of mass cytometry data with bead standards. Cytometry A 2013;83(5):483–494. doi:10.1002/cyto.a.22271, PMID:23512433.

[38] Kotecha N, Krutzik PO, Irish JM. Web-based analysis and publication of flow cytometry experiments. Curr Protoc Cytom 2010;Chapter 10:Unit10.17. doi:10.1002/0471142956.cy1017s53, PMID:20578106.

[39] Nowicka M, Krieg C, Crowell HL, Weber LM, Hartmann FJ, Guglietta S, *et al*. CyTOF workflow: differential discovery in high-throughput high-dimensional cytometry datasets. F1000Res 2017;6:748. doi:10.12688/f1000research.11622.3, PMID:28663787.

[40] Chen H, Lau MC, Wong MT, Newell EW, Poidinger M, Chen J. Cytofkit: A Bioconductor Package for an Integrated Mass Cytometry Data Analysis Pipeline. PLoS Comput Biol 2016;12(9):e1005112. doi:10.1371/journal.pcbi.1005112, PMID:27662185.

[41] Levine JH, Simonds EF, Bendall SC, Davis KL, Amir el-AD, Tadmor MD, *et al*. Data-Driven Phenotypic Dissection of AML Reveals Progenitor-like Cells that Correlate with Prognosis. Cell 2015;162(1):184–197. doi:10.1016/j.cell.2015.05.047, PMID:26095251.

[42] Becht E, McInnes L, Healy J, Dutertre CA, Kwok IWH, Ng LG, *et al*. Dimensionality reduction for visualizing single-cell data using UMAP. Nat Biotechnol 2019;37:38–44. doi:10.1038/nbt.4314, PMID:30531897.
[43] Cohen J. A power primer. Psychol Bull 1992;112(1):155–159. doi:10.1037//0033-2909.112.1.155, PMID:19565683.
[44] Storey JD, Tibshirani R. Statistical significance for genomewide studies. Proc Natl Acad Sci U S A 2003;100(16):9440–9445. doi:10.1073/pnas.1530509100, PMID:12883005.
[45] Benjamini Y, Hochberg Y. Controlling the false discovery rate: a practical and powerful approach to multiple testing. J R Stat Soc B (Methodol) 1995;57(1):289–300. doi:10.1111/j.2517-6161.1995.tb02031.x.
[46] Shen W, Song Z, Zhong X, Huang M, Shen D, Gao P, *et al*. Sangerbox: A comprehensive, interaction-friendly clinical bioinformatics analysis platform. Imeta 2022;1(3):e36. doi:10.1002/imt2.36, PMID:38868713.
[47] Zhang Z, Zhang S, Zou Z, Shi J, Zhao J, Fan R, *et al*. Hypercytolytic activity of hepatic natural killer cells correlates with liver injury in chronic hepatitis B patients. Hepatology 2011;53(1):73–85. doi:10.1002/hep.23977, PMID:21254163.
[48] Schuch A, Hoh A, Thimme R. The role of natural killer cells and CD8(+) T cells in hepatitis B virus infection. Front Immunol 2014;5:258. doi:10.3389/fimmu.2014.00258, PMID:24917866.
[49] Deaglio S, Zubiaur M, Gregorini A, Bottarel F, Ausiello CM, Dianzani U, *et al*. Human CD38 and CD16 are functionally dependent and physically associated in natural killer cells. Blood 2002;99(7):2490–2498. doi:10.1182/blood.v99.7.2490, PMID:11895784.
[50] Le Bouteiller P. Human decidual NK cells: unique and tightly regulated effector functions in healthy and pathogen-infected pregnancies. Front Immunol 2013;4:404. doi:10.3389/fimmu.2013.00404, PMID:24324468.
[51] Wherry EJ. T cell exhaustion. Nat Immunol 2011;12(6):492–499. doi:10.1038/ni.2035, PMID:21739672.
[52] Bogacka J, Pawlik K, Ciapała K, Ciechanowska A, Mika J. CC Chemokine Receptor 4 (CCR4) as a Possible New Target for Therapy. Int J Mol Sci 2022;23(24):15638. doi:10.3390/ijms232415638, PMID:36555280.
[53] Wang Y, Zhang Y, Yang X, Han W, Liu Y, Xu Q, *et al*. Chemokine-like factor 1 is a functional ligand for CC chemokine receptor 4 (CCR4). Life Sci 2006;78(6):614–621. doi:10.1016/j.lfs.2005.05.070, PMID:16137713.
[54] Möbs C, Salheiser M, Bleise F, Witt M, Mayer JU. Basophils control T cell priming through soluble mediators rather than antigen presentation. Front Immunol 2022;13:1032379. doi:10.3389/fimmu.2022.1032379, PMID:36846020.
[55] Atri C, Guerfali FZ, Laouini D. Role of Human Macrophage Polarization in Inflammation during Infectious Diseases. Int J Mol Sci 2018;19(6):1801. doi:10.3390/ijms19061801, PMID:29921749.
[56] Zhang YH, He M, Wang Y, Liao AH. Modulators of the Balance between M1 and M2 Macrophages during Pregnancy. Front Immunol 2017;8:120. doi:10.3389/fimmu.2017.00120, PMID:28232836.
[57] Suhail M, Abdel-Hafiz H, Ali A, Fatima K, Damanhouri GA, Azhar E, *et al*. Potential mechanisms of hepatitis B virus induced liver injury. World J Gastroenterol 2014;20(35):12462–12472. doi:10.3748/wjg.v20.i35.12462, PMID:25253946.